Effects of surface preparation on bond behavior CFRP-to-PA6 bonded joints using different adhesives

Manel Dallali, Marco Gigliotti, Eric Lainé, Jean-Claude Grandidier, Nicolas Henry

Version of Record: https://www.sciencedirect.com/science/article/pii/S0360319921029062
Manuscript_48ed944d2aab9598b5d408e98f461ac7

Effects of surface preparation on bond behavior CFRP-to-PA6 bonded joints using different adhesives

Manel Dallali[1], Marco Gigliotti[1], Eric Lainé[1], Jean-Claude Grandidier[1], Nicolas Henry[2]

[1]Institut Pprime (UPR CNRS 3346-ISAE-ENSMA-Université de Poitiers), Department of Physics and Mechanics of Materials, 1 Avenue Clement Ader, F-86961 Chasseneuil Futuroscope, France.

[2]RESCOLL, Société de Recherche, 8 Allée Geoffroy Saint-Hilaire, CS 30021, F-33615 Pessac, France.

Abstract

This paper focuses on an experimental study of the explosive decompression on representative samples of the hyperbaric type IV hydrogen storage vessels. The adhesion of the composite to the liner is achieved by different adhesives. The bond behavior of liner-to-composite bonded joint considerably depends on the properties of adhesives, as well as the assembly process. X-ray tomography allows determining the damages before and after explosive decompression tests. Tomographic observations have revealed a certain level of porosity due to the assembly process with plasma treatment. This porosity influences the damage mechanisms induced by explosive decompression. Results show that 1) the increasing of the maximum hydrogen pressure (differential pressure induced during the depressurization step between the liner/adhesive interface or the adhesive/composite) increases the risk of liner collapse for the same gas exposure conditions, 2) Compared with soft adhesive, the stiff adhesive has proven better adhesion between the composite and the liner, 3) the flame treatment improved the surface energy of the PA6 and subsequently increased the collapse limit pressure, 4) adhesive RCA-20 with plasma preparation can be defined as a kind of low strength to collapse adhesive with a collapse limit pressure less than 2 MPa, 5)adhesive RCA-2000 with flame treatment can be defined as a kind of high strength to collapse adhesive in the present report with a collapse limit pressure between 15 MPa and 17.5 MPa.

Keywords: Liner collapse, Hydrogen, Explosive decompression, adhesives

1 Introduction

Hydrogen gas, owing to the advantages of renewability and producing harmless by products, has gained sufficient attention as a source of eco-friendly energy [1]. To get a good economy of hydrogen, three main points to consider: the production of hydrogen, the storage of

hydrogen and the further development of the hydrogen fuel cells [2]. Fuel cell vehicles (FCVs) have developed rapidly in recent years from both technological and business perspectives[3], because of the cleanliness and wide availability of hydrogen and the high energy efficiency of FCVs [4–6]. In this context, the onboard hydrogen storage methods for FCVs and the hydrogen storage in general plays a crucial role. There are different ways to store hydrogen, such as liquid (cryogenic) storage tanks [7], polymer and composite foams [8], metal hydrides [9], gaseous high-pressure storage vessels [10]. Some companies have developed composite-type high-pressure vessels made of an aluminum or plastic liner to limit the leak, reinforced with the carbon fiber layer outside of the liner to support the pressure. The last generation of these vessels, known as type IV, which consists of a polymer liner is commonly used for hydrogen storage. Composite high-pressure tanks are now a mature way of storing hydrogen it is used by automotive company and gas producers.

To satisfy the industry's specifications such as volumetric hydrogen density, the internal pressure can reach in service a pressure equal to 70 MPa. The level of pressure imposes necessarily to use the carbon fiber layer outside. Many researchers [11–14] studied simulation and burst experiments on 70 MPa type IV hydrogen storage vessels and show the capabilities of carbon fiber solution. In articles [15–19] authors have studied the damage behavior of hydrogen storage vessel composites to ensure safety.

As far as the liner is concerned, different solutions are proposed depending on the service conditions (temperature, tolerated leakage rate) but also on the process used to manufacture the tank. Polyamide PA6 due to its strong molecular polarity and hydrogen bond interaction limiting the permeability has gradually become the potential choice for type IV hydrogen storage tank in contrast to other polymers and the high permeability of polyethylene [20–23].

However, feedback from experience in the use of these vessels reveals several problems. A crack between liner and composite can appear during in-service life. For example, Yersak et al. [24] studied the blistering of liners in a type IV tank for hydrogen storage to keep the liner safe. Pepin et al. [20] and Blanc-Vannet et al. [21] studied the liner collapse phenomenon. This collapse phenomenon demonstrated experimentally during rapid emptying of tanks, consists of a detachment and a significant deformation of the liner [27]. More precisely when the pressure suddenly drops the dissolved gases in the materials (liner composite glue) generate a crack at the composite-liner interface that eventually propagates. The onset of crack could be the consequence of the coalescence of small bubbles, but it is just an assumption because this one has never been proved.

Pepin et al. [28] studied specifically the liner-composite collapse due to the phase of decompression on thermoplastic plates. The samples used by Pepin et al. [28] are prepared by thermo-compression of a stack of one composite layer and a polymer liner layer. The pressure and temperature applied during the curing cycle allow bonding between composite and liner. To achieve this, the liner and composite are joined by an adhesive applied just before the winding operation, which is intended to allow the molecular chains of the liner to bond with the thermosetting resin of the composite. An open question that has not been addressed in the literature concerns the correlation between the performance of the adhesive and the resistance to explosive decompression. This is the subject of this article. The study focuses on a high-pressure type IV (hydrogen) tank consisting of an inner shell called a polymer liner on which the carbon fibers impregnated with a thermosetting resin are wound. But, due to the important cost of type IV vessels and the difficulty to work at high hydrogen pressure, the experimental study will be realized as in Pepin's work [20, 23], on a representative sample composed of an assembly of thermoplastic polymer and composite plates bonded together by different adhesive formulation and surface preparation.

In the context of a massive deployment of hydrogen tanks, it is essential to ensure the best sustainability of all systems that constitute the energy chain and to evaluate new concepts. More precisely, the present paper aims to quantify the resistance of the assembly to fast decompression as a function of the different glue formulations having different physical and mechanical properties. The increase of the property of adhesive and the liner-composite assembly performances purpose is to delay the collapse phenomenon during explosive decompression. However, the samples tested are plates square made by a layer of liner and composite materials assembled with different glues. The assemblies have been obtained by compression. These explosive decompression experiments were performed, at the same temperature and emptying rate but at different maximum hydrogen pressure, thanks to a tensile testing machine equipped with a high-pressure chamber.

A complementary study with X-rays allows determining the defect of the assemblage and the damages suffered by the sample during the decompression step. X-ray tomography images will be subject to segmentation and image processing procedures developed to quantify the damaged surface.

2 Materials and experimental procedures

Due to the important cost of tests performed on hyperbaric type IV hydrogen storage vessels, an experimental design based on a representative sample is used to reproduce the debonding and deformation of the inner liner of hyperbaric hydrogen storage vessels during the decompression step. The materials used in this study have been supplied as they are equivalent to the ones used in industrial applications.

2.1 Materials

The assemblies are composed of a 2 mm-thick composite material layer on which is fixed by an adhesive a 2 mm-thick molded sheet of polymer liner. The PA6 liner material used in this work was PA6 raw material produced by RÖCHLING SE and Co. KG. PA6 is bonded, using an adhesive, to carbon fiber reinforced polymer (CFRP) composites plates, produced by Hexcel. The material property of CFRP is listed in Table 1. PA6 is characterized by Differential Scanning Calorimetry (DSC) under nitrogen atmosphere at 10 °C.min^{-1} and displays a glass transition temperature at 40.4 °C, which is in agreement with the literature [29]. Samples are square of 60x60 mm of these 4 mm-thick multi-layered materials.

PA6 liner								
Young's modulus E (MPa)			Poisson's coefficient ν			Yield stress σ_y(MPa)		
3200			0.4			80		
Composite								
Young modulus			Poisson coefficients			Shear modulus		
E_{11}(MPa)	E_{22}(MPa)	E_{33}(MPa)	ν_{12}	ν_{13}	ν_{23}	G_{12}(MPa)	G_{13}(MPa)	G_{23}(MPa)
72000	72000	8000	0.36	0.38	0.8	4500	4500	2800
Adhesive								
	Target Young's modulus (MPa)		Traction tests Young's modulus (MPa)			DMA tests E' (MPa) @ 21°C@ 1Hz	Glass transition temperature Tg (°C)	
RCA-20	10		8.5			11.72	-45	
RCA-2000	2000		3471			2316	68	

In the tank, the assembly between the liner and the composite is assured by an adhesive deposited just before the winding operation. Here a glue layer is deposed on the surface and the PA6 plate is linked with the carbon epoxy plate by pressure. The glue is applied with a brush spatula to the carbon epoxy plate surface, after that the PA6 plate is deposited and a pressure is used to ensure a good assembly. The aim is to enable the molecular chains of the liner to be bonded with the thermosetting resin of the composite. New formulations of adhesives have been generated with different morphological specificities. More specifically, two adhesives that exhibit different Young's modulus (à 23 °C) have been used in the stacking:

- Soft adhesive (RCA-20) with an expected Young's module (E) of 10 MPa: this one leads to a better homogeneity of stress in the joint, even with lower ultimate stress before failure
- Stiff adhesive (RCA-2000) with an expected Young's module 2000 MPa a value lower than that of the E-modulus of PA6.

To characterize these adhesives, bulk adhesive specimens were manufactured (cure in a mould) with the dimensions that the standard ISO 527-2 [30]. Five samples for each adhesive were tested under tensile loading, at room temperature, and with a speed of testing of 1 mm/min. The properties of adhesives resulting from the dynamic mechanical analysis, according to the standard practice ASTM E1640 on the DMA facility, METRAVIB DMA 100, and differential scanning calorimetry (DSC) tests are summarized in Table 1.

The measured Young's modulus of RCA-20 and RCA-2000 were 8.5 MPa and 3471 MPa, respectively. Concerning RCA-20 Young's modulus of adhesives is reduced greatly to the target value and higher of expected value for RCA-2000. The DMA modulus are slightly different but give an evaluation of Young's modulus at 65 °C (temperature of decompression tests) 2 MPa for RCA 20 and 1599 MPa for RCA 2000.

2.2 Processing of the bonded samples

A large number of industrial fields use structural bonding for their applications today and this technique depends on the bonding process (surface treatment, curing, pressure...) which is specific to each industry. During the manufacture of the tanks, the thermoplastic liner is covered with a chemical element that promotes the bonding with the thermosetting composite.

The samples used in this study are representative of the industrial structure. However, a specific preparation protocol adapted to the adhesives is implemented.

There are three basic steps for proper PA6 surface preparation: degreasing, abrading, and plasma or flaming treatment. Depending on the condition of the surface, abrasion cleaning, solvent cleaning or both may be necessary. The degreaser used for PA6 is Isopropyl Alcohol. For proper removal, abrasion cleaning (sandpaper P400) is required to obtain acceptable adhesion. In this study, two recommended preparations have been selected to prepare the samples (Table 2):

- Atmospheric plasma treatment: The use of plasma treatment to treat polymers has been known for more than 20 years. Atmospheric plasma treatment works at atmospheric pressure and with air, which is electrically conductive and consists of excited atoms, ions, and free radicals. This allows polymer surfaces to be cleaned, or chemically modified [31].
- Flame treatment: Surface treatment by gas flame is a simple, rapid, effective, and economical method of improving the surfaces of a wide range of plastics. Among all the influential factors, the thickness of the adhesive layer has an important effect on the mechanical properties of the adhesive joint [32]. For that, calibration glass beads were added in process 2. It should be noted that 1% in weight of glass beads, concerning the mass of glue, doesn't change adhesion properties.

	Process 1	**Process 2**
Composite surface preparation	Peel-ply	Peel-ply
Polymer surface preparation	plasma treatment	flame treatment
Glass beads in the adhesive	ø	150µm

The surface free energy, which plays a key role in the adhesion of two surfaces, can be divided into the dispersion part γ^d and the polar part γ^p as presented in Equation (1).

$$\gamma = \gamma^d + \gamma^p \quad (1)$$

The surface free energy of the samples with different surface treatments was calculated using a Dataphysics OCA-30 contact angle analyzer (Figure 1). Three test liquids with known surface tensions were used as the probe liquids for the contact angle measurement, including distilled water, diiodomethane, and ethylene glycol.

Surface free energy and its components obtained experimentally are shown in Table 3. The surface energy of PA6 influences adhesion onto the composite [33]. To improve the adhesion force to substrates, it is common to use flame or plasma treatments that introduce polar groups onto the surface [34]. The flame treatment increases slightly the polar surface energy of PA6.

	γ	γ^d	γ^p
IPA degreasing	51.6	42.5	9.1
Plasma treatment	64	40.6	23.4
Flaming treatment	63.6	33.9	29.7

Figure 1: System of surface energy measurement

2.3 Experimental setup

Decompression tests were carried out in an Instron 8802 hydraulic tensile machine (Figure 2) fitted with a pressure and temperature regulated chamber enabling mechanical testing in gaseous hydrogen (H_2) up to 40 MPa. The first step aims at purging the ambient air from the pressure cell. Three nitrogen purges were systematically performed up to 1 MPa after closing the chamber.

This study is carried out at 65 °C, to reach faster the equilibrium state by increasing the permeation rate of hydrogen, which increases with increasing temperature [35]. The temperature increased rapidly during the pressure ramp and gradually returned to equilibrium, aided by the circulation of water around the chamber and load cell. Once the sample is thermally stable, the maximum H_2 pressure (Pmax) is applied inside the chamber at a constant rate of 1 MPa/min. In fact, for H_2, which is a slightly soluble gas, it was shown that the permeability coefficient increases with temperature whereas it varies slightly when hydrogen pressure rises [36]. A final time of 7 days was chosen to ensure a fully saturated sample. Once fully saturated with Hydrogen, depending on the test conditions, samples are subjected to

rapid decompression of 5 MPa/min as illustrated in Figure 3. This decompression rate is selected following a study carried out by Pepin et al. [25] which shows even while multiply by 10 at this rate, the size or amplitude of the collapses do not increase.

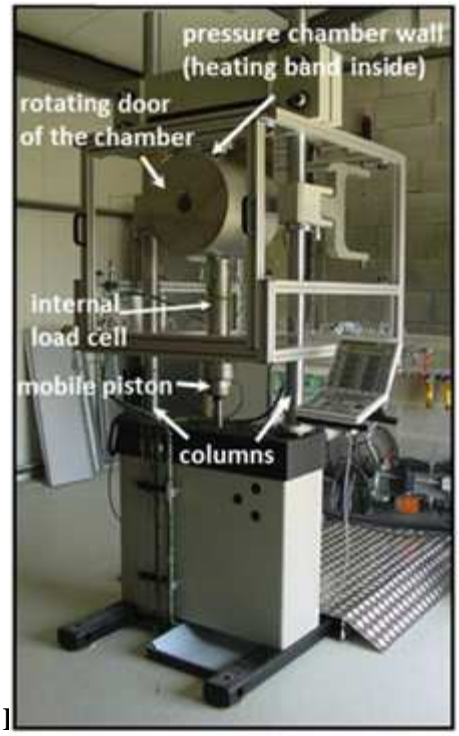

] [23]

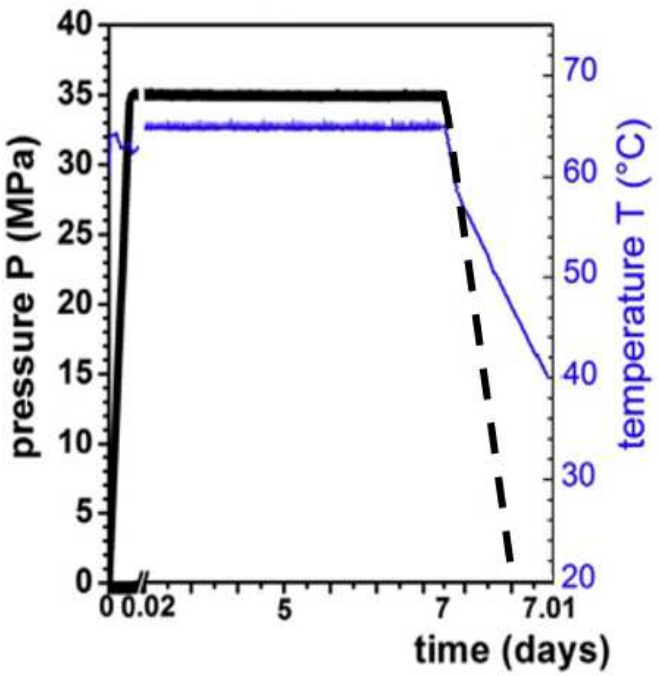

Figure 3: Temperature and pressure evolution during a decompression test

The working pressures of the tanks are 35 MPa and can reach 70 MPa, as far as rapid decompression is concerned, the occurrence of damage depends on: the pressure level and the decompression speed. If the system used can only reach 35 MPa, the speed can be fast enough to generate damage.

2.4 Microscopy and tomography observations

First, the samples are observed on their edge with an optical microscope to evaluate the thickness and regularity of the adhesive layer. X-Ray tomography scans are performed to evaluate the initial defect in the glue layer and at the interface liner/composite.

Secondly, to evaluate the collapsed area after decompression, both observation techniques are considered, the optic which allows, thanks to the transparency of the liner, to assess the collapsed area. However, this technique is restricted to 2D for that, X-Ray tomography observations were made both before and after explosive decompression tests to estimate the

volume of defects. To identify the kind of adhesive joint failure after explosive decompression, optical observations make it by focusing on the cross-section of the specimen.

2.4.1 Microscopic observations

The morphology and thickness distribution of the adhesive are determined by optical microscopy on 15 mm long piece cut from the specimen is embedded in a potting resin. The cross-sectional area was polished using sandpapers (P1000. P2000. P4000) and afterward polished with a 1 µm diamond suspension. This cross-section has been observed with the Alicona 3D InfiniteFocus imaging microscope using 10×, 20×, and 50× magnification objectives with vertical resolutions of 100, 50, and 20nm, respectively, and a lateral resolution of 1.76, 0.88, and 0.46 µm, respectively.

2.4.2 µ-tomographic observations

X-ray Computed Tomography has become an increasingly popular technique owing to its non-destructive and non-invasive technique used to investigate the microstructure of an object based on the attenuation coefficient of the electromagnetic wave such as an X-ray [37]. The micro-tomography scans of this study were obtained with the UltraTom CT scanner manufactured by RX-Solutions [38]. The X-ray tomography imaging technique was used to visualize the 3D architecture of the composite/adhesive/liner as well as the different defects present in the virgin sample and after the test. To save time, four samples were observed with a resolution of 28 µm/voxel. A complete analysis, lasting 5 h, is made by acquiring a considerable number (2000 in our case) of X-ray absorption radiographs of the same sample under different viewing angles.

Image pre-processing is necessary to reduce the impact of image artifacts such as noise, image blur, beam hardening, ring effects, and bright spots [39]. This is achieved by the application of image filters like median, mean, non-local mean, and edge detecting filters that help improve the quality of reconstructed raw images and prepare them for image segmentation.

2.4.3 X-Ray images analysis - segmentation

Image segmentation is a key step in many applications in pattern recognition, computer vision, and image understanding to allow further image content exploitation y efficiently [40]. The final architecture of the material and collapse were determined from the segmentation of tested specimens. Segmentations are done with Avizo segmentation editor [41] that facilitates

operations on composite materials. Thus, image segmentation assigns voxels to one of the groups: composite, liner, adhesive, or air (collapse). Cropping the data is useful to exclude the outside of the specimen. A crop editor is provided for this purpose. Collapses are then segmented by selecting all the pixels of the peak of the histogram that corresponds to the collapse. Once the collapse was segmented, its volume percentage was calculated by dividing the total volume of collapse by the total volume of the sample.

The accuracy of the segmentation output was assessed visually by comparing segmented slices with the corresponding original images.

3 Results and discussion

This section begins with a report on the initial state of samples by focusing on the faults linked to the assembly. To compare the different configurations, a study on the collapse limit pressure was carried out. To understand the characteristics of adhesive joint failure, it is necessary to study each of the failure modes. The final architecture of the samples with collapses was determined from segmentation.

3.1 Initial state

Porosity is one of the typical defects found in bonded specimens, which could represent a critical defect.

Figure 2: Tomographic observations of porosity in the adhesive for plasma treatment (RCA-2000) (a) XZ plane - (b) XY plane - (c) XY plane

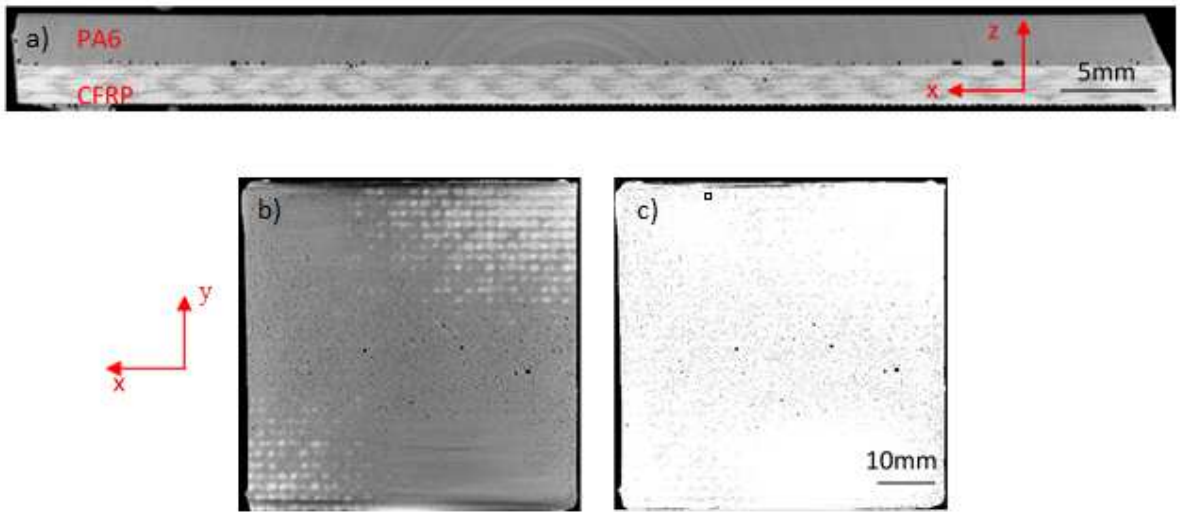

The tomography observations for plasma treatment (Figure 4.a and 4.b) show a high level of porosity. This porosity was measured at the liner/composite interface. The porosity is represented in the form of black circles with varied sizes in Figure 4. The surface percentage of the porosity in the sample was measured by a computer-aided measurement technique: implemented within FIJI-ImageJ [42]. Raw input images were preprocessed manually to reduce background noise and enhance the apparent brightness. The next step of the ImageJ protocol, the thresholding technique employed to images to segment collapse (Figure 4.c). Finally, the percentage value of collapse was calculated using the command Analyze > Measure. The volume percentages of porosities at the interface are respectively equal to 3.8% and 3.2% for adhesive RCA-20 and RCA-2000. The distribution is uniform and, often, the

size is coherent with the glue thickness. It was generally reported that the strength of the assembly decreases with the increasing porosity [43].

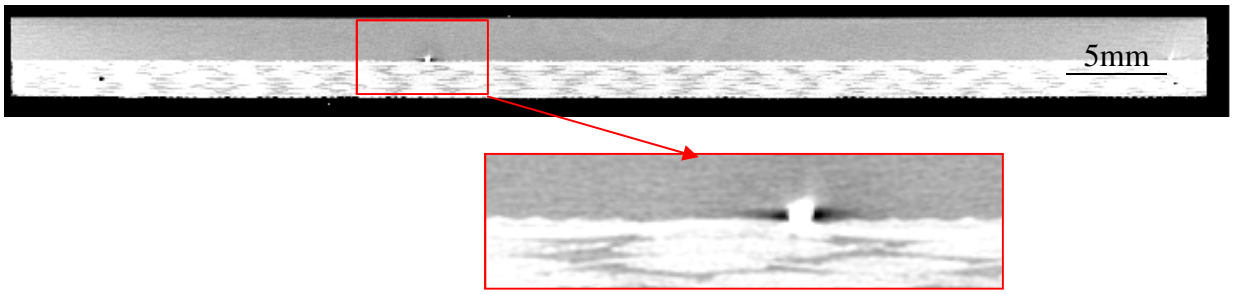

Figure 3 :Tomographic observations of glass beads in the adhesive for flame treatment

The tomography observations for the second process (flame treatment) (Figure 5) show the glass beads used to calibrate the thickness of the glued joints. Glass beads are represented in the form of white circles of 100-200 µm diameter. Glass beads are systematically surrounded by air bubbles which are represented by black spots and have indented the PA6 surface. Consequently, they are not effective in assuring a good thickness calibration of the joint. Despite the aspect of the few tomographic images showing some pores of relatively big dimensions, the measurement of volume percentages shows that the global level of porosity is negligible compared to plasma treatment. The distribution on the surface is not uniform, but no clusters have been observed (Figure 6).

Comparing the two processes, differences in the thickness of the glue joint are noticeable. On the other hand, the thicknesses are homogeneous, which is consistent with the tomography. For the thickest glue joints, the pores have a diameter of the same order of magnitude as the thickness. To quantify in the following, the effect of the thicknesses of the adhesive, the measures gave for plasma treatment 3 mm and 3.2 mm for RCA-20 and RCA-2000 respectively, and for flame treatment, 0.07 and 0.04 mm for RCA-20 and RCA-2000 respectively.

	RCA-20	RCA-2000

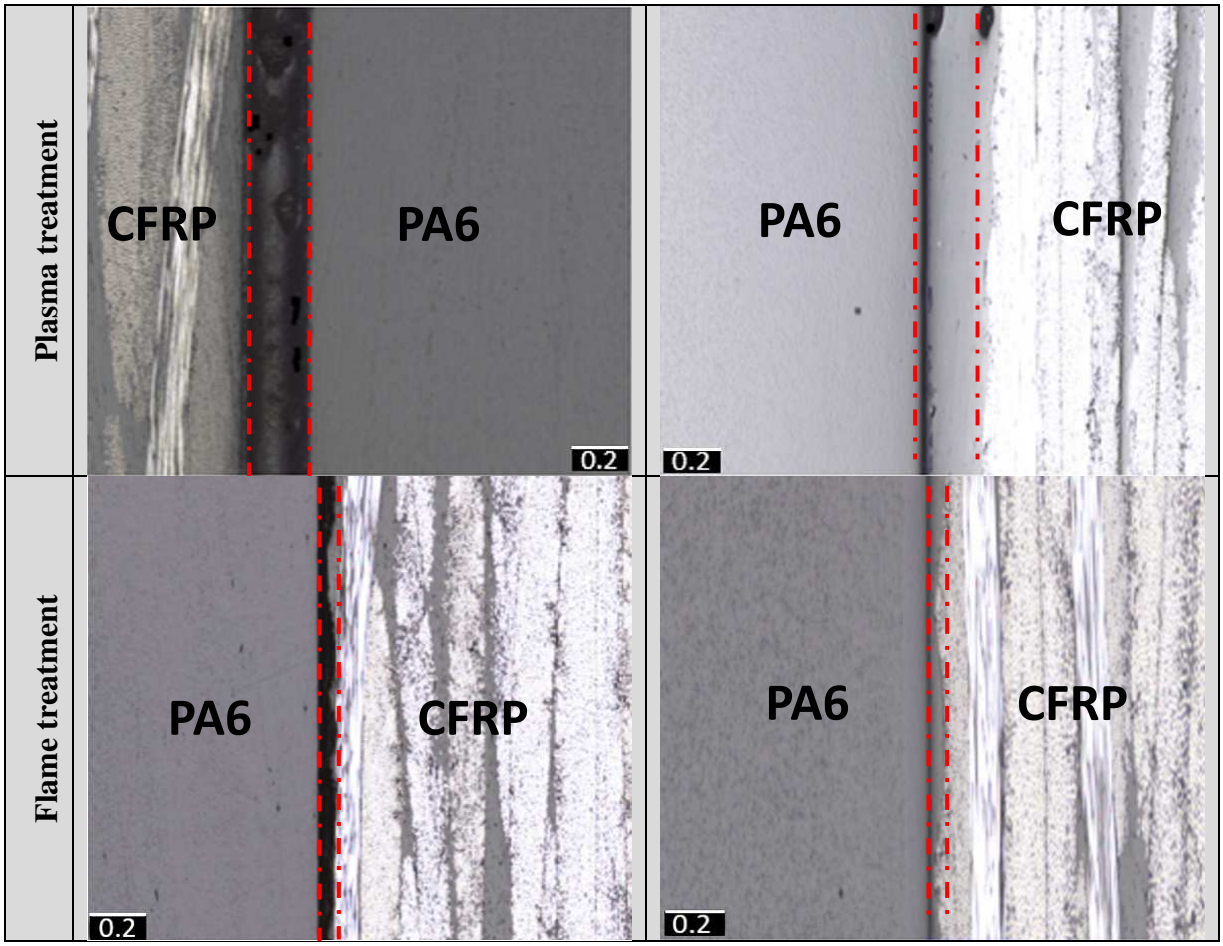

Figure 6 : Microscopic observation of the edge of samples (mm)

The results of measurements show a difference in thicknesses between different samples. The objective principle of the addition of the glass beads is to have a homogeneous thickness between the samples. The tomography observations confirm this functionality. Because of the effect of the mechanical behavior of the liner and CFRP, the glass beads did not succeed has to obtain the desired objective.

3.2 Collapse limit pressure for different samples

Let us recall that all the tests are carried out at 65 °C on separate specimens. At 65 °C and for an emptying rate of 5 MPa.min^{-1}, tests, carried out on plates assembled without adhesive but following with a chemical treatment (confidential), have given collapse limit pressure between 31 MPa and 35 MPa [28]. During the stabilization step, the hydrogen dissolved in the materials and build up between the composite and the liner. The time of this step was chosen to ensure a fully saturated sample for a test performed at 65 °C and for a given hydrogen pressure. The temperature and the decompression rate are identical for all tests to compare the different systems. Before obtaining the collapse limit pressure value of hydrogen, the tests are

carried out only once. To have a confirmation of the limit collapse pressure values, the explosive decompression tests with these pressure are repeated twice.

At this maximal saturation pressure of 35 MPa applied to the specimens for enough time to reach a homogeneity of the dissolved hydrogen concentration, all the specimens present more or less important collapses. When for each type of assembly, saturation is achieved at lower pressures as defined in Table 4, the phenomenon no longer appears for these specific conditions.

The limit in saturation pressure is directly dependent on the type of adhesive and surface treatment. This confirms that the mechanism depends on the intrinsic properties of the adhesive where the phenomenon starts and on the strength properties of the assembly which certainly facilitates or slows down the propagation of the collapse. The surface energy ensuring the cohesion of the stack is one of the important parameters in the degradation phenomenon. Table 4 shows the presence (numerical value defined after) or absence (NC) of collapse as a function of the type of adhesive and the type of treatment.

It is also important to underline that for all the cases where a collapse appears, it intervenes after the end of the return to the ambient pressure. As in the previous studies, the delay time is observed. Unfortunately, apart from the sound generated by a sudden collapse, it has not been possible to follow and measure this degradation time with precision. In standard operating conditions of vessels, the time required to empty, related to the emptying flow rate, is much faster than hydrogen time desorption from the materials. These conditions are also the same during these explosive decompression experiments. For that, collapse appears during the draining step.

As far as the RCA-20 adhesive material is concerned, the plasma treatment did not avoid the collapse that appears at all pressures, on the other hand, the flame treatment improved the assembly because it takes 3.5 MPa of saturation pressure to generate a debonding.

The most rigid material RCA-2000 presents much more interesting capacities, the collapses appear for pressure values between 7.5 MPa and 15 MPa for the assembly prepared with the plasma technique and between 10 MPa and 17.5 MPa by the one treated by flame.

Flame treatment delays the collapse resistance and the stiffness of the adhesive is a major parameter in the resistance to collapse as it has been demonstrated in massive elastomer-type materials [44].

3.3 Mode of failure

After the decompression test, microscope images of the failure surfaces of the CFRP adherent and the liner were taken and analyzed to characterize the failure patterns (Figure 7).

For surface treatment with plasma, an adhesive failure appears (black band between the two lines in red), the failure takes place at the adhesive/PA6 interface. After surface treatment of PA6 with flaming, the decompression test leads to the collapse of type the adhesive failure, but in this case, the adhesive remains attached to the composite. The flame treatment introduces polar groups to the surface of PA6, increasing adhesion.

No correlation was found between the areas of the presence of cavities and the development of the collapse, in other words after the collapse, some areas with defects remain assembled. Knowing that the sizes of the observed porosities are homogeneous and their distribution is uniform.

It is also important to emphasize that collapse occurs in the core and that possible edge stress concentrations do not participate in the mechanism.

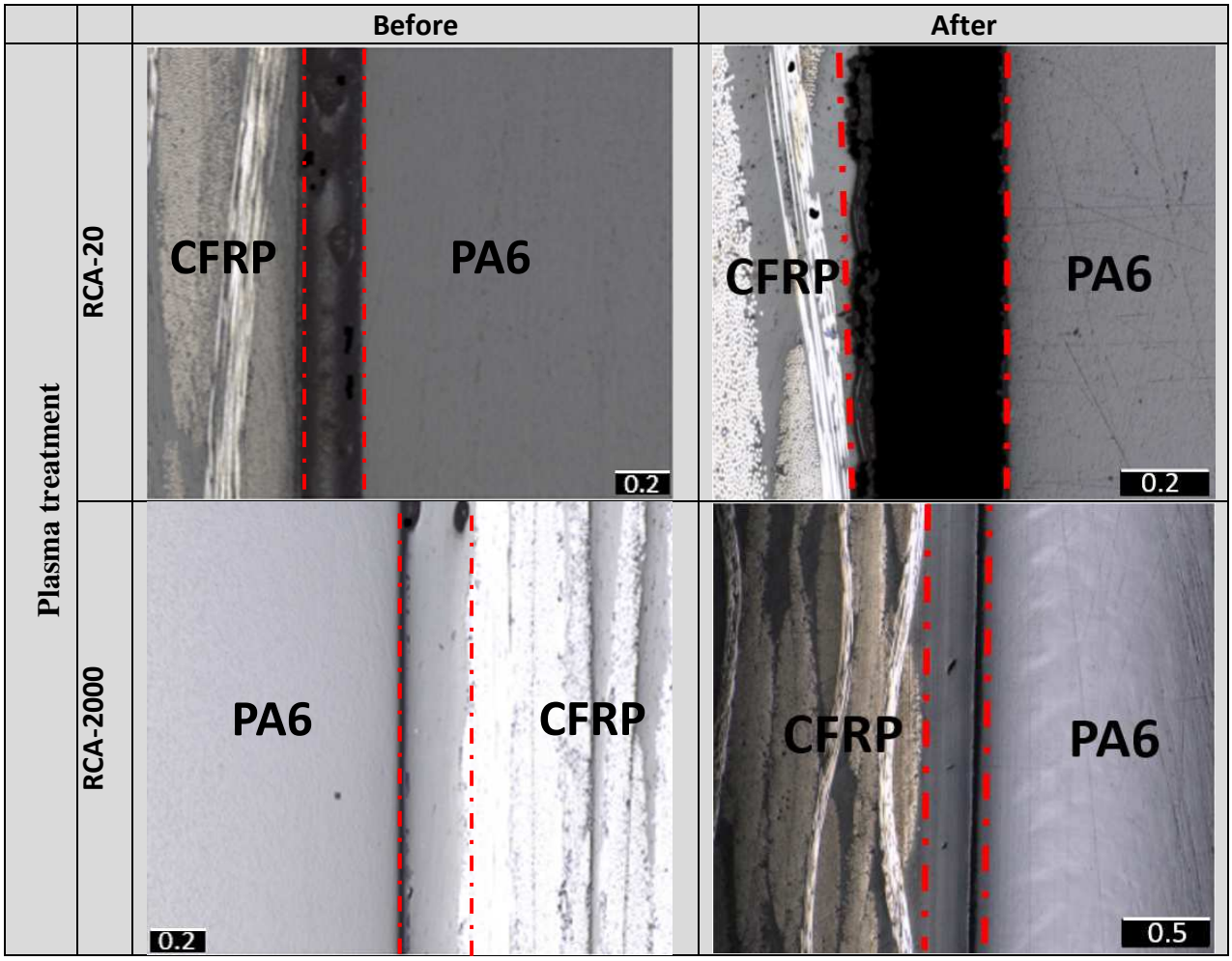

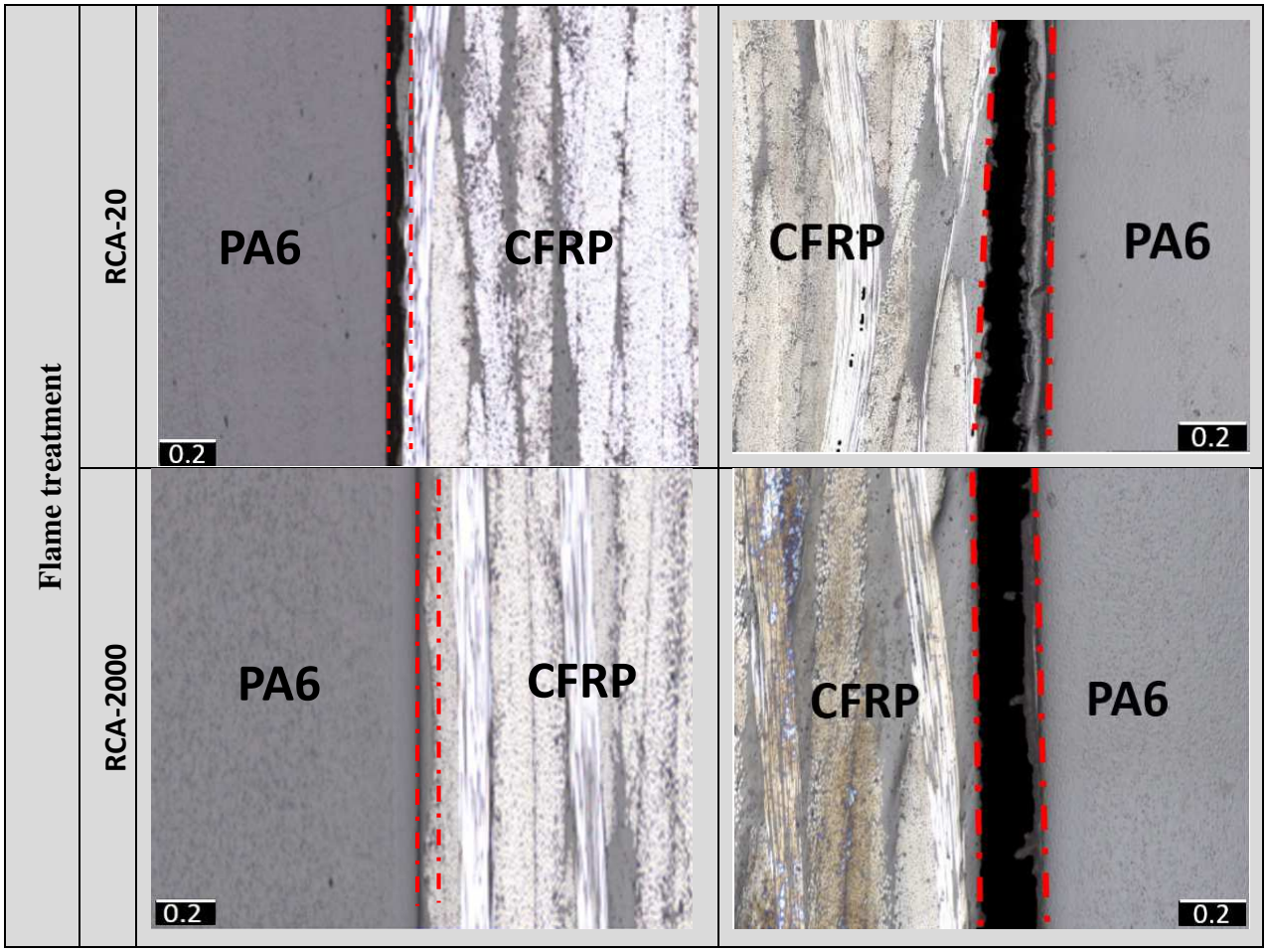

Figure 7 :Adhesives thicknesses (mm)

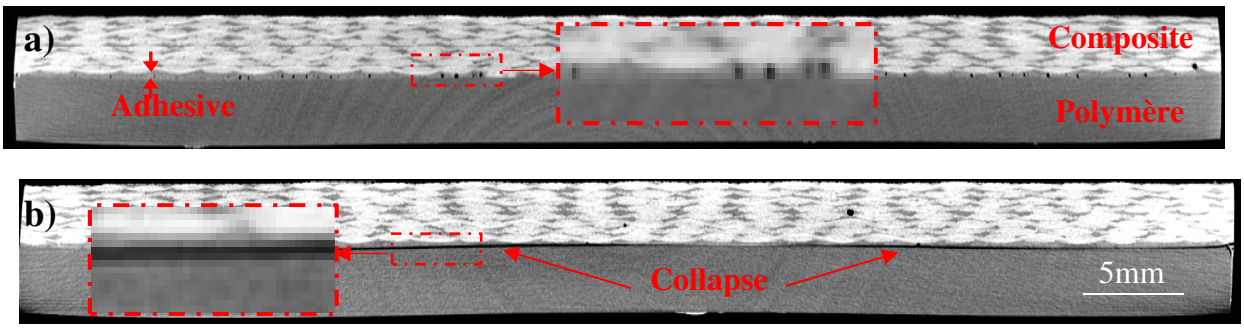

Figure 4: Tomography of the cross-section : (a) initial state - (b) after explosive decompression test (plasma treatment RCA - 2000)

3.4 Analysis of surface segmentation

The initial architecture of the material and collapse were determined from the segmentation of specimens tested, and a specific procedure was applied to retrieve collapse created by explosive decompression. The comparison of tomographic views at the PA6/composite interface performed both before and after the explosive decompression test (Figure 8), shows

the appearance collapses take place between PA6 and composite although the two materials are well glued in their initial state (Figure 8.a).

The final architecture of the material and collapse were determined from the segmentation of tested specimens. Thus, image segmentation assigns voxels to the air (collapse and porosity). Using X-ray computed tomography alongside simple and accurate image segmentation methods allows the detection and measurement of collapse. This information is one of the essential data for the understanding and assessment of the effect of different test parameters on adhesion performance.

To illustrate the different phases to be segmented (Composite, liner, collapse, glass beads, porosity), a particular 2D slice of sample is shown in Figure 8 with the selected range of the corresponding grey values histogram (Figure 9).

One can see in Figure 9 that there are three well-differentiated peaks. The first peak corresponds to the collapse, the porosity, and the exterior air. The densities of the liner and the resin of composite material are very similar their grey levels are all included in the second peak. The third peak represents well yarns of composite material and glass beads. Adhesives have grey values that are very closer to those of the liner (light grey) for that, the identification is not straightforward.

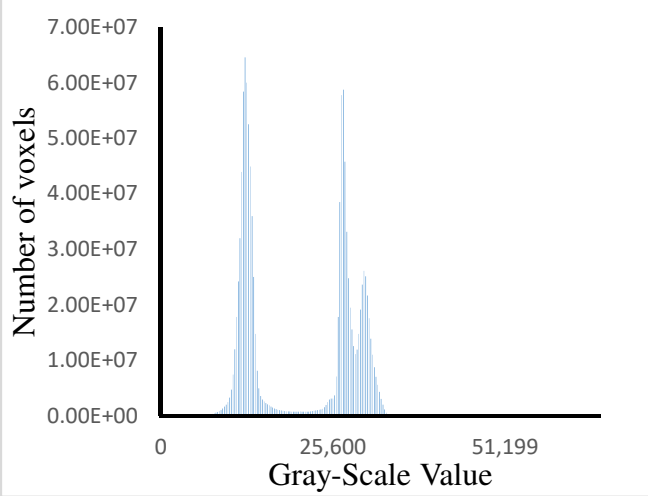

Figure 9: Histogram of gray values

It is important to keep in mind that, although X-ray Tomographic can facilitate characterizing the material internal geometry, quantitative evaluation of these defects depends on the spatial resolution and tomography images noise [45], and the reliability of the obtained results is

directly related to the quality of tomography scans and the segmentation process parameters [46].

Two thresholding methods can be applied for image segmentation - 3D and 2D thresholding. The 3D segmentation is based on X-ray computed tomography images. The images used in 2D segmentation were captured with a high-resolution Digital Camera.

The segmentation step is performed semi-automatically. Thresholding methods are not straightforward and usually lead to segmentation errors that need to be manually corrected by the operator, thus involving a time-consuming procedure. The thresholding is carried out by manually adjusting the threshold mark between the phases. The raw, as well as segmented images of plates, are compared to demonstrate the validity of the approach.

As an example, Figure 10 shows the reconstructed slice that is extracted from the 3D picture of the sample prepared with plasma treatment after the explosive decompression test. Computed tomography images are obtained and segmented using a simple thresholding procedure. Starting from the segmented image, it is possible to detect collapses.

The collapsed areas are represented by white areas on the real image of the plate (Figure 10.a) and by red zones on the segmentation result (Figure 10.b). Due to the negligible thickness of the collapse generated by the explosive decompression tests, the very small collapses remained unnoticed in the reconstructed image. When the collapse width is closer to the voxel size, the collapse gray levels appear to be intermediate between those of the adhesive and the liner or composite. The porosities present in the initial state of the plate are not visible in the results of segmentation. It can be concluded that the adopted segmentation procedure is unable to deliver meaningful results.

Figure 5: (a) Original image by camera - (b)Segmentation performed using 3D tomographic reconstructions of samples prepared with plasma treatment (RCA-2000)

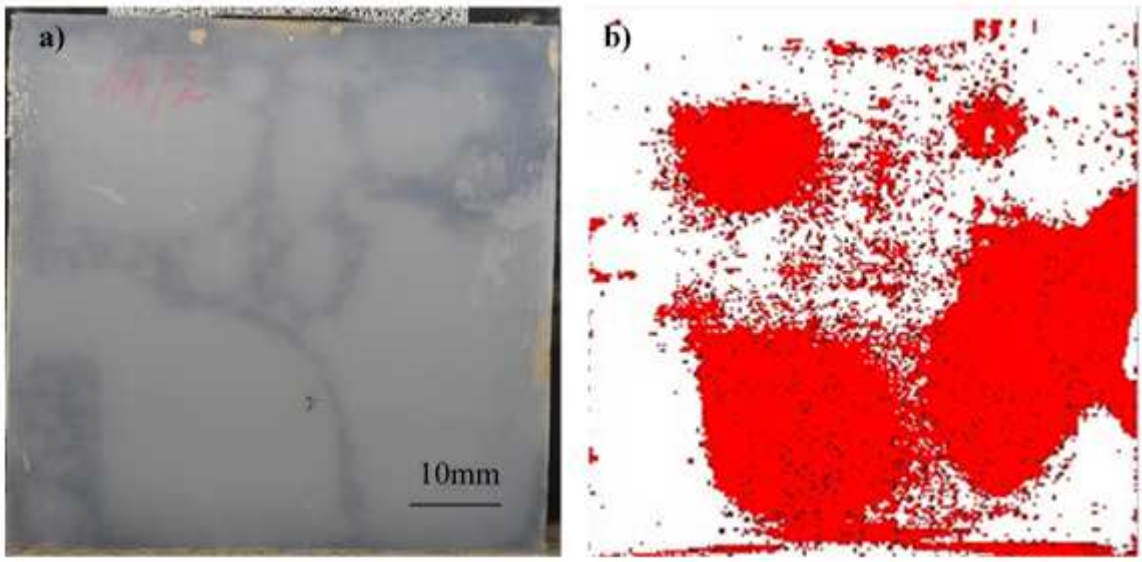

Figure 6: (a) Original image by camera - (b) Segmentation performed using 3D tomographic reconstructions of samples prepared with flame treatment (RCA-2000)

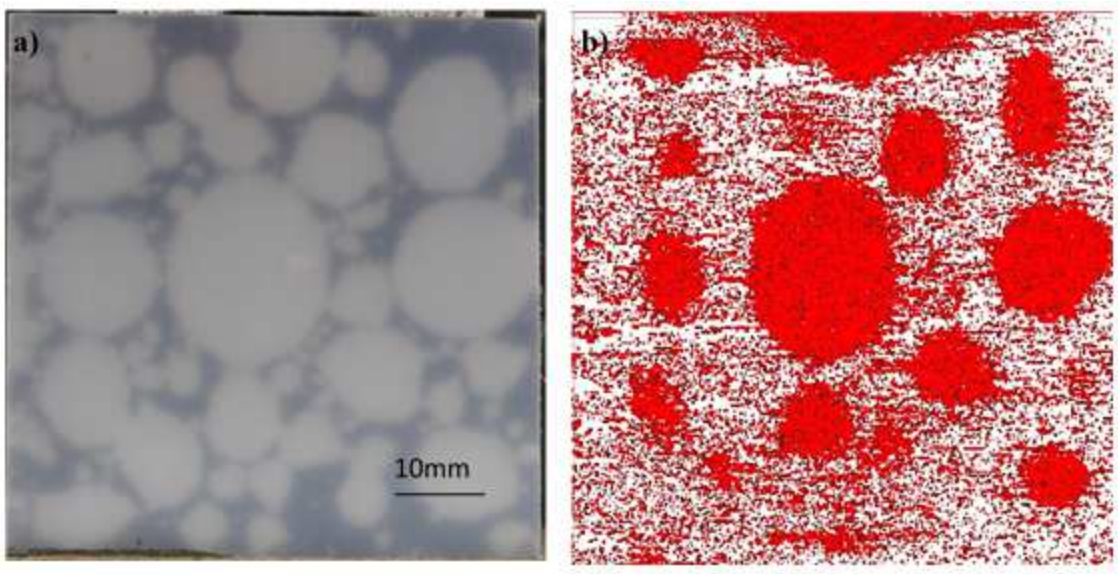

Figure 11 shows one of the results of 3D segmentation for the sample prepared with flame treatment after the explosive decompression test. Glass beads were well distributed throughout the adhesive. Due to some tomography artifacts and the presence of glass beads in segmented images, additional difficulties in the damage reconstruction processes happened.

The images used in 2D segmentation were captured with a high-resolution digital Camera (Figure 12.a). Figure 12.b illustrates the segmentation result starting from the initial image. The collapse, represented by the clear isolated regions (Figure 12.a), is easier to recognize and is consequently successfully segmented.

By comparison of the two images in Figure 12, in the 2D segmented image, the identification of the various phases was consistent with visual identification from the original image. The results showed an excellent correlation in terms of the collapse's shape, dimensions, and distribution. The adopted segmentation procedure leads to good results. 2D image segmentation showed better performance compared with 3D tomographic images. This performance is only adapted for the RCA-2000 adhesive thanks to its transparency, on the other hand, it is not valid for the RCA-20 adhesive which makes the collapses not visible.

Figure 7: (a) Original image by camera - (b) 2D slice example of collapses segmentation

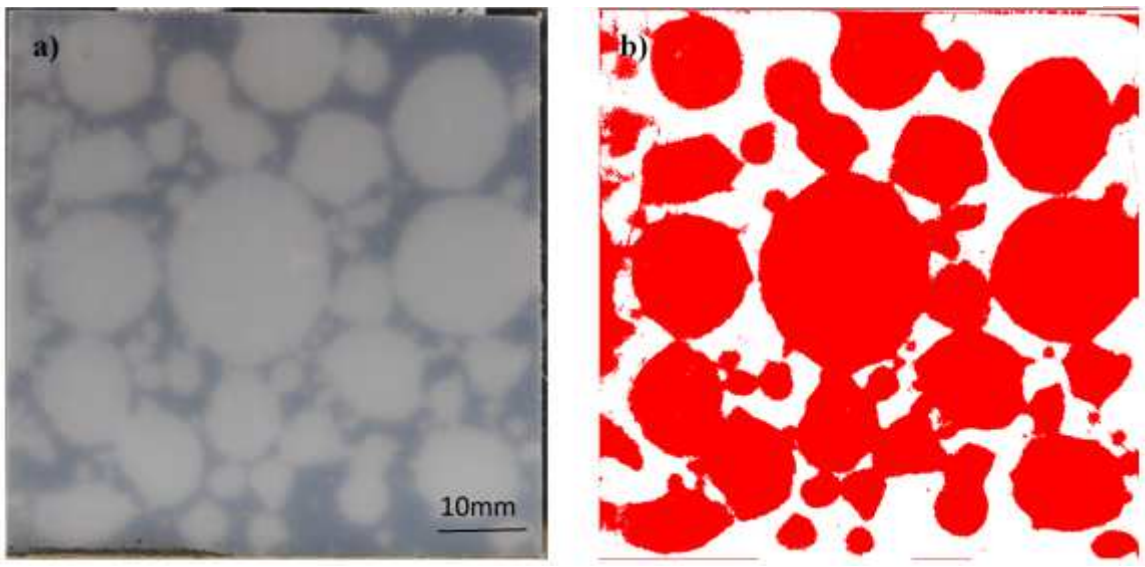

3.5 Correlation between the obtained results

The results of quantification of collapses, dynamic E-modulus by DMA, and Tg measurement by DSC for adhesives, as well as the collapse presu pressure, are listed in Table 4.

Tomographic measurements were performed for various explosive decompression applied to the samples, it is possible to apply the porosity percentage technique, to evaluate the final size of collapse depending on the explosive decompression tests. It should be noted that the porosity presented in Table 4 is expressed as relative percentages of the total volume of adhesive in the sample with 3D tomography observations. Due to the negligible thickness of the collapse generated by the explosive decompression tests, the very small collapses remained unnoticed in the reconstructed image which causes errors in the volume percentage of collapse measured. On the other hand, due to the effort of opening residual important in certain samples, some collapses have an upper thickness as those of the adhesive, which gives a percentage greater than 100% if the volume of the collapse is related to the volume of the glue. This report was therefore not retained. Equally, the collapse is quantified by the percentage of porosity in the plates relative to the total area of the sample.

Compared with 3D segmentation, the results of 2D segmentation provided better measurements for collapses, but this method was not adapted for RCA-2000 adhesives which are not transparent. Analysis and crossing of these results lead to an understanding of interface fracture mechanisms and therefore leads to fruitful conclusions of how to choose the best adhesive/ adherent system.

Table 4: Results of all tests (TD: Total debonding, CLP: Collapse limit pressure, NC: No collapse)

	Plasma treatment on PA6		**Flame treatment on PA6**	
	RCA-20	**RCA-2000**	**RCA-20**	**RCA-2000**
Bulk glue properties				
E(MPa) 21°	8.5	3471	8.5	3471
E'(MPa) 65°	2	1599	2	1599
E'(MPa) 21°	11.72	2316	11.72	2316
Tg(°C)	-45	68	-45	68
Assembly				
Adhesive thickness (mm)	0.3	0.32	0.07	0.04
Glass beads(mm)	No	No	Yes	Yes

Porosity %	3.8	3.2		≃0	≃0	
Delamination localization	PA6 / glue	PA6 / glue		M77 / glue	M77 / glue	
Pressure applied (MPa)	% collapse volume	% collapse volume	% collapse area	% collapse volume	% collapse volume	% collapse area
2	15.77	NC	NC	NC	NC	NC
3.5	22.22	NC	NC	20.4	NC	NC
5	14.05	NC	NC	13.26	NC	NC
7.5	18.78	NC	NC	TD	NC	NC
10	8.31	2.7	58.4	TD	NC	NC
17.5	11.32	6.21	68.24	TD	20.05	38.8
25	13.04	5.265	66.13	TD	100	58.67
35	15.77	13.5	70.61	TD	100	73.78
CLP (MPa)	<2	7.5-10		2-3.5	15-17.5	

According to the collapse limit pressure, the type of adhesives is the first parameter responsible for the liner collapse. The value of CLP for RCA-2000 is 5 times as much as that for RCA-20 for the two surface treatments considered. We find the same results on elastomeric gaskets whose link between stiffness and resistance to collapse has been described in the literature, for example, Gent et al. [47]. More the stiffness is important more the limit of pressure is high. Therefore it seems advisable to choose a stiff bond between the layers.

Next, attention was directed towards examining the effect of PA6 surface treatment on the nature of assemblies as a function of pressure in explosive decompression tests. Flame treatment improves the adhesion qualities of polymers. With flame-treated surfaces, bond strength and durability are much improved. The value of the CLP is doubled in moving from plasma treatment to flame treatment. Regarding the initiation of the phenomenon, it seems difficult to separate the effect of initial defects or the presence of glass beads from the quality of the interface. However, it is important to note that the pores generated in the case of the use of the plasma manufacturing process have the size of the thickness and nothing could explain that these bubbles privilege one or the other interface. Moreover, we have not observed a

correlation between the distribution of initial porosity and the presence of the glass beads with the position or the size of collapses. To evaluate the effect of stiffness and the presence of initial bubbles, further tests must be carried out.

The increase in the saturation pressure leads to an increase in the differential in the pressure induced during the depressurization step between the inside and the outside of the sample. This differential of pressure plays a key role in the onset and propagation of collapse, which explains the increase in the debonding area with the increase in the pressure for RCA-2000 assemblies. If the strength of the link influences the level of limit pressure, the propagation is a balance between the internal pressure of solved gas and interfacial energy. For example for a percent of collapse area equal to 58%, it is necessary to apply 15 MPa additional for damage the assembly with flame treatment in comparison to plasma treatment. For soft glue, the flame treatment permits to support 3.5 MPa, whereas with the plasma treatment it is lower than 2 MPa.

The local properties of glue and the strength of the interface play a major role in the onset of damage. As the stiffness depends on Tg the influence of temperature can de indirect, it is important to underlying this fact because the tank should be used in many situations. For a car, the range of temperature is -50 °C to 90 °C. Consequently, the deviation from the glass transition temperature is a major parameter for the specification of the adhesive.

To summarize, adhesive RCA-20 with plasma preparation can be defined as a kind of low strength to collapse adhesive, and adhesive RCA-2000 with flame treatment can be defined as a kind of high strength to collapse adhesive in the present report. This indicated that the relatively higher tensile strength adhesive led to PA6 delamination with more pressure compared to lower tensile strength adhesive.

4 Conclusions

This report presents a detailed study of the effect of adhesive properties and assembly processes on the bond strength of a composite-liner bonded multilayer by performing a series of explosive decompression tests under H_2. X-ray tomography and microscopic observations conducted on the samples before and after the explosive decompression allowed to quantify the geometry of the adhesive layer, the manufacturing defects, and the size of the damage created by the explosive decompression. The latter takes place either at the liner or composite adhesive interface depending on the surface treatment applied to the liner. The limiting pressure values are strongly dependent on the stiffness and surface treatment, the

quantification of the role played by the initial defects is an issue to be addressed to evaluate the order of importance of the parameters in the collapse mechanism. A correlation of different characteristics with the pressure limit led to the following findings:

(1) The stiffness of the adhesive is the main parameter responsible for the liner collapse. A higher modulus of elasticity of the adhesive increases the limit pressure of collapse occurrence in the specific configurations of this test.

(2) Surface energy, which is related to the surface treatment, is the second major parameter in the collapse phenomenon both concerning its propagation and its position in the assembly, a flame treatment has improved the performance of the structure.

(3) The thickness of the adhesive and the porosity of the samples seems to have less influence on the occurrence of the collapse phenomenon but this point needs to be confirmed.

Acknowledgements

This study was conducted within the framework of the project “Increase of Strength of Interface Between liner and composite in HYdrogen tank (ISIBHY)” (project 5127) which has been funded with the support from the French National Centre for Scientific Research (CNRS) and from the Regional Council of Nouvelle-Aquitaine. This work was partially funded by the French Government program “Investissements d'Avenir” (EQUIPEX GAP, reference ANR-11-EQPX-0018). Pprime Institute gratefully acknowledges "Contrat de Plan Etat - Région Nouvelle-Aquitaine" (CPER) as well as the "Fonds Européen de Développement Régional (FEDER)" for their financial support to the reported work.

Reference

[1] Zhang Q, Xu H, Jia X, Zu L, Cheng S, Wang H. Design of a 70 MPa type IV hydrogen storage vessel using accurate modeling techniques for dome thickness prediction. Compos. Struct. 2020;236: 111915. https://doi.org/10.1016/j.compstruct.2020.111915.

[2] Khzouz M, I. Gkanas E. Hydrogen Technologies for Mobility and Stationary Applications: Hydrogen Production, Storage and Infrastructure Development. In: Al Qubeissi M, El-kharouf A, Serhad Soyhan H, editors. Renewable Energy - Resources, Challenges and Applications, IntechOpen; 2020. https://doi.org/10.5772/intechopen.91676.

[3] Zhao L, Zhao Q, Zhang J, Zhang S, He G, Zhang M, et al. Review on studies of the emptying process of compressed hydrogen tanks. Int. J. Hydrog. Energy 2021;46:22554–73. https://doi.org/10.1016/j.ijhydene.2021.04.101.

[4] Veziroglu TN. In Assessment of hydrogen energy for sustainable development. 21st Century's energy: Hydrogen energy system. 2007:9-31. Springer, Dordrecht..

[5] Forsberg P, Karlstrom M. On optimal investment strategiesfor a hydrogen refueling station. Int J Hydrogen Energy 2007;32:647-60. https://doi.org/10.1016/j.ijhydene.2006.05.018
[6] Maus S, Hapke J, Ranong C, Wuchner E, Friedlmeier G, Wenger D. Filling procedure for vehicles withcompressed hydrogen tanks. Int J Hydrogen Energy 2008;33:4612-21. https://doi.org/10.1016/j.ijhydene.2008.06.052
[7] Ifju P, Myers D, Schulz W. Residual stress and thermal expansion of graphite epoxy laminates subjected to cryogenic temperatures. Compos. Sci. Technol. 2006;66:2449–55. https://doi.org/10.1016/j.compscitech.2006.02.011.
[8] Lévesque S, Ciureanu M, Roberge R, Theodore Motyka. Hydrogen storage for fuel cell systems with stationary applications-I. Transient measurement technique for packed bed evaluation. Int. J. Hydrog. Energy 2000;25:1095-1105. https://doi.org/10.1016/S0360-3199(00)00023-9
[9] Banyay GA, Shaltout MM, Tiwari H, Mehta BV. Polymer and composite foam for hydrogen storage application. J. Mater. Process. Technol. 2007;191:102-05. https://doi.org/10.1016/j.jmatprotec.2007.03.074
[10] Villalonga S, Nony F, Magnier C, Yvernes JL, Thomas C, Delmas B, et al. Composite 700 bar-vessel for on-board compressed gaseous hydrogen storage. In Proc. of 17th International conference on composite materials; July.2009. Edinburgh, UK.
[11] Leh D, Saffré P, Francescato P, Arrieux R, Villalonga S. A progressive failure analysis of a 700-bar type IV hydrogen composite pressure vessel. Int. J. Hydrog. Energy 2015;40: 13206-14. https://doi.org/10.1016/j.ijhydene.2015.05.061
[12] Leh D, Magneville B, Saffr P, Villalonga S. Optimisation of 700 bar type IV hydrogen pressure vessel considering composite damage and dome multi-sequencing. Int. J. Hydrog. Energy 2015;40: 13215-30. https://doi.org/10.1016/j.ijhydene.2015.06.156
[13] Ramirez JPB, Halm D, Grandidier J-C. 700 bar type IV high pressure hydrogen storage vessel burst-Simulation and experimental validation. Int. J. Hydrog. Energy 2015;40: 13183-92. https://doi.org/10.1016/j.ijhydene.2015.05.126
[14] Magneville B, Gentilleau B, Villalonga S, Nony F, Galiano H. Modeling, parameters identification and experimental validation of composite materials behavior law used in 700 bar type IV hydrogen high pressure storage vessel. Int. J. Hydrog. Energy 2015;40: 13193-13205. https://doi.org/10.1016/j.ijhydene.2015.06.121
[15] Ramirez JPB, Halm D, Grandidier JC, Villalonga S. A fixed directions damage model for composite materials dedicated to hyperbaric type IV hydrogen storage vessel - Part I: Model formulation and identification. Int. J. Hydrog. Energy 2015;40:13165-73. https://doi.org/10.1016/j.ijhydene.2014.08.071
[16] Ramirez JPB, Halm D, Grandidier JC, Villalonga S. A fixed directions damage model for composite materials dedicated to hyperbaric type IV hydrogen storage vessel - Part II: Validation on notched structures. Int. J. Hydrog. Energy 2015;40:13174-82. https://doi.org/10.1016/j.ijhydene.2015.06.014
[17] Zu L , Xu H, Wang H, Zhang B, Zi B. Design and Analysis of Filament-wound Composite Pressure Vessels Based on Non-geodesic Winding. Compos. Struct. 2019;207:41:52. https://doi.org/10.1016/j.compstruct.2018.09.007
[18] Zu L, Koussios S, Beukers A. A novel design solution for improving the performance of composite toroidal hydrogen storage tanks. Int. J. of Hydrog. Energy 2012;37:14343-50. https://doi.org/10.1016/j.ijhydene.2012.07.009
[19] Zu L, Koussios S, Beukers A. Design of filament–wound domes based on continuum theory and non-geodesic roving trajectories. Compos. Part A Appl. Sci. Manuf. 2010;41:1312-20. https://doi.org/10.1016/j.compositesa.2010.05.015

[20] Klopffer MH, Berne P, Weber M, Castagnet S, Hochstetter G, Espuche E. New materials for hydrogen distribution networks: materials development and technico-economic benchmark. In Defect and Diffusion Forum 2012;323:407-12. https://doi.org/10.4028/www.scientific.net/DDF.323-325.407
[21] Dao DQ, Trung Q, Nang D, Luche J, Rogaume T, Richard F, et al. Polyamide 6 and Polyurethane Used as Liner for Hydrogen Composite Cylinder: An Estimation of Fire Behaviours. Fire Technol. 2014;52:397-420. https://doi.org/10.1007/s10694-014-0423-4
[22] Chernev BS, Eder GC. Side effects in the application of polyamide 6 barrier materials for fuel tanks. J. Appl. Polym. Sci 2013;127:230-36. https://doi.org/10.1002/app.37868
[23] Kumar SS, Kanagaraj G. Investigation on Mechanical and Tribological Behaviors of PA6 and Graphite-Reinforced PA6 Polymer Composites. Arab J Sci Eng 2016;41:4347-57. https://doi.org/10.1007/s13369-016-2126-2
[24] Yersak TA, Baker DR, Yanagisawa Y, Slavik S, Immel R, Mack-Gardner A, et al.. Predictive model for depressurization-induced blistering of type IV tank liners for hydrogen storage. Int. J. Hydrogen. Energy 2017;42:28910e7. https://doi.org/10.1016/j.ihydene.2017.10.024
[25] Pepin J, Lainé E, Grandidier JC, Benoit G, Mellier D, Weber M, et al. Replication of liner collapse phenomenon observed in hyperbaric type IV hydrogen storage vessel by explosive decompression experiments. Int. J. Hydrog. Energy 2018;43:4671-80. https://doi.org/10.1016/j.ijhydene. 2018.01.022
[26] Blanc-Vannet P, Papin P, Weber M, Renault P, Pépin J, Lainé E, et al. Sample scale testing method to prevent collapse of plastic liners in composite pressure vessels. Int. J. Hydrog. Energy 2019;44: 8682-8691. https://doi.org/10.1016/j.ijhydene.2018.10.031
[27] Yuan L, Kyriakides S. Liner wrinkling and collapse of bimaterial pipe under axial compression. Int J Solids Struct 2015;60-61:48-59. https://doi.org/10.1016/j.ijsolstr.2015.01. 029
[28] Pepin J, Lainé E, Grandidier JC, Castagnet S, Blanc-Vannet P, Papin P, Weber M. Determination of key parameters responsible for polymeric liner collapse in hyperbaric type IV hydrogen storage vessels. Int. J. Hydrog. Energy 2018;43:16386-99. https://doi.org/10.1016/j.ijhydene.2018.06.177
[29] Greco R, Nicolais L. Glass transition temperature in nylons. Polymer 1976;17:1049–53. https://doi.org/10.1016/0032-3861(76)90005-7.
[30] ISO 527-2 :2012, « Plastiques – détermination des propriétés en traction – Partie 2 : Conditions d'essai des plastiques pour moulage et extrusion ».
[31] Molitor P, Barron V, Young T. Surface treatment of titanium for adhesive bonding to polymer composites: a review. Int J of Adhesion and Adhesives 2001;21:129-136. https://doi.org/10.1016/S0143-7496(00)00044-0
[32] Liao L, Huang C, Sawa T. Effect of adhesive thickness, adhesive type and scarf angle on the mechanical properties of scarf adhesive joints. Int J Solids Struct 2013;50:4333–40. https://doi.org/10.1016/j.ijsolstr.2013.09.005.
[33] Zhao B, Kwon HJ. Adhesion of Polymers in Paper Products from the Macroscopic to Molecular Level — An Overview. J Adhes Sci Tech 2011;25:557–79. https://doi.org/10.1163/016942410X525821.
[34] Madeira DMF, Vieira O, Pinheiro LA, de Melo Carvalho B. Correlation between Surface Energy and Adhesion Force of Polyethylene/Paperboard: A Predictive Tool for Quality Control in Laminated Packaging. Int. J. Chem. Eng. 2018;2018:1–7. https://doi.org/10.1155/2018/2709037.
[35] Klopffer MH, Flaconnèche B. Transport Properties of Gases in Polymers: Bibliographic Review. Oil Gas Sci. Technol. 2001;56:223-44. ttps://doi.org/10.2516/ogst:2001021

[36] Naito Y, Kamiya Yosh, Terada K, Mizocuchi Ke, Wang JS. Pressure dependence of gas permeability in a rubbery polymer. J. Appl. Polym. Sci. 1996;61:945-50.https://doi.org/10.1002/(SICI)1097-4628(19960808)61:6<945::AID-APP8>3.0.CO;2-H.
[37] Sarkar G, Siddiqua S. Effect of fluid chemistry on the microstructure of light backfill: An X-ray CT investigation. Eng. Geol. 2016;202:153-62. https://doi.org/10.1016/j.enggeo.2016.01.012
[38] « RX Solutions, UltraTom XL: Ultra High Performance 3d Nano Ct System ». Available: http://www.rxsolutions.fr/ct-systems [Accessed 12 December 2017].
[39] Purswani P, Karpyn ZT, Enab K, Xue Y, Huang X. Evaluation of image segmentation techniques for image-based rock property estimation. J. Pet. Sci. Eng. 2020;195:107890. https://doi.org/10.1016/j.petrol.2020.107890
[40] Frucci M, Di Baja GS. From Segmentation to Binarization of Gray-level Images. Pattern Recognit 2008;3:1-13. https://doi:10.13176/11.54
[41] Avizo 9.0, 2015. FEI Visualization Sciences Group.
[42] imagej.net/Fiji.
[43] Mugica GW, Tovio DO, Cuyas JC, González AC. Effect of Porosity on the Tensile Properties of Low Ductility Aluminum Alloys. Mater. Res. 2004;7:221-29. https://doi.org/10.1590/S1516-14392004000200002
[44] Jaravel J, Castagnet S, Grandidier JC, Gueguen M. Experimental real-time tracking and diffusion/mechanics numerical simulation of cavitation in gas-saturated elastomers. Int. J. Solids Struct 2013;50:1314-1324. https://doi.org/10.1016/j.ijsolstr.2013.01.001
[45] Tiseanu I, Tsitrone E, Kreter A, Craciunescu T, Loarer T, Pégourié B, Dittmar T. X-ray micro-tomography studies on carbon based composite materials for porosity network characterization. Fusion Eng. Des. 2011;86:1646-51. https://doi.org/10.1016/j.fusengdes.2011.04.079
[46] Madra A, El Hajj N, Benzeggagh M. X-ray microtomography applications for quantitative and qualitative analysis of porosity in woven glass fiber reinforced thermoplastic. Composites Sci. Technol. 2014;95:50-58. https://doi.org/10.1016/j.compscitech.2014.02.009
[47] Gent A, Tompkins D. Nucleation and growth of gas bubbles in elastomers. Int. J. Appl. Phys. 1969;40:2520-25. https://doi.org/10.1063/1.1658026.